Interaction of the explosive molecules RDX and TATP with IRMOF-8

ARTICLE *in* THE JOURNAL OF PHYSICAL CHEMISTRY C · MAY 2010

Impact Factor: 4.77 · DOI: 10.1021/jp906192g

3 AUTHORS:

Khorgolkhuu Odbadrakh
Joint Institute for Computational Sciences,...
34 PUBLICATIONS **106** CITATIONS
SEE PROFILE

James P Lewis
West Virginia University
90 PUBLICATIONS **2,796** CITATIONS
SEE PROFILE

Donald Nicholson
University of North Carolina at Asheville
234 PUBLICATIONS **2,188** CITATIONS
SEE PROFILE

Interaction of the Explosive Molecules RDX and TATP with IRMOF-8

Khorgolkhuu Odbadrakh* and James P. Lewis†

Department of Physics and Astronomy, West Virginia University, Morgantown, West Virginia 26506

Donald M. Nicholson

Computer Science and Mathematical Division, Oak Ridge National Laboratory, Oak Ridge, Tennessee 37831

Received: July 1, 2009; Revised Manuscript Received: March 18, 2010

We report our investigations on physisorption and trapping of high explosive (HE) molecules 1,3,5-trinitro-*s*-triazine or cyclotrimethylene trinitramine (RDX) and triacetone triperoxide (TATP) by an isoreticular metal−organic framework (IRMOF) IRMOF-8. In general, IRMOFs are known for their high porosity and tailorability, thus having potential applications as preconcentrators, and gas storage. In particular, IRMOF-8 has higher hydrogen uptake than the extensively studied IRMOF-1, thus having the potential to act as preconcentrators for explosive molecules. We employed the ab initio density functional theory (DFT) code FIREBALL to estimate physisorption interactions for the RDX and TATP molecules with interior and exterior surfaces of IRMOF-8. At zero temperature, RDX yields several physisorption type binding configurations, while TATP remains more inert to interactions with IRMOF-8. Molecular dynamics simulations at room temperature result in trapping configurations preferring TATP inside the IRMOF-8 cage, which could be attributed to molecular sieving effects.

I. Introduction

Isoreticular metal−organic frameworks (IRMOFs) are crystalline compounds of metal clusters (connectors) bridged by organic molecules (linkers) and having periodic topology extending in three dimensions. IRMOFs have attracted a lot of interest recently for their potential use in a range of technologies such as hydrogen storage, sensors, gas separation, and photonics.[1−5] Various design strategies for synthesizing IRMOFs for specific applications have been proposed and tested.[6−8] One potentially high impact application of IRMOFs is to use it as a selective preconcentrator of explosive molecules for detection purposes.[9] Conventional detection technologies use zeolites and carbon based preconcentrators, which are not very selective and have a low absorbent to weight mass ratios of around 1%. Detecting trace amount of explosives using these conventional preconcentrators requires exposing a large amount of absorbent to a target air environment for extended period of time, which translates into longer response time and higher cost. High internal surface area (1000−5400 m^2/g), robust mechanical properties at temperatures 300−400 °C, and tailorable structural scaffolding make IRMOFs an ideal candidate for a highly efficient preconcentrator for explosives.[10,11]

In this paper, we mainly focus on physisorptions of two common high explosive (HE) molecules cyclotrimethylene trinitramine (RDX) and triacetone triperoxide (TATP) (Figure 1a,b) by IRMOF-8 (Figure 2a,b). IRMOF-8 has 2,6-naphthalenedicarboxylate (NDC group) linkers (Figure 2c) and Zn_4O tetrahedron connectors (Figure 2b) and represents simple variation of IRMOF-1, the most studied metal organic framework. Thanks to its NDC linkers, IRMOF-8 provides up to 4 times as many adsorption sites and steep initial adsorption for hydrogens[12] than IRMOF-1. RDX is commonly used in military and industry as a component of C4 plastic explosives and was used in the terrorist attack on the USS Cole in Yemen in 2000. TATP is used by terrorists in numerous attacks including the 2001 attempted attack by the shoe bomber. A typical scenario

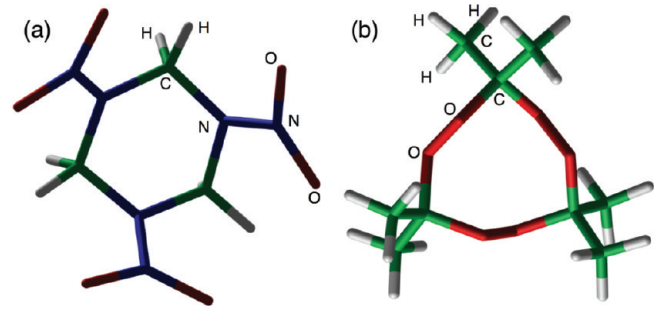

Figure 1. (a) 1,3,5-Trinitro-*s*-triazine (RDX) and (b) TATP.

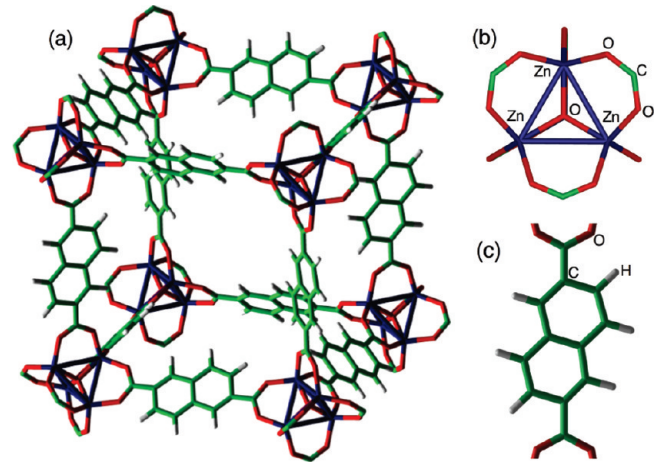

Figure 2. (a) IRMOF-8 cage, (b) its connector, and (c) 2,6-naphthalenedicarboxylate (NDC) linker.

* Corresponding author. Electronic address: od.odbadrakh@mail.wvu.edu.
† Electronic address: james.lewis@mail.wvu.edu. URL: http://fireball.phys.wvu.edu/LewisGroup/.

10.1021/jp906192g
Published on Web 04/14/2010

in these kind of situations is that the HEs would be concealed well enough so that only a trace amount of the explosives is present in its immediate environment. Therefore, the availability of highly sensitive and rapid detection technologies based on molecular sensing is paramount. IRMOFs are one of the most promising materials for selective explosive preconcentrators.

In general, gas adsorption by porous materials is characterized by one or several of the following mechanisms:[3,13,14] molecular sieving effect caused by size and/or shape exclusion; thermodynamic equilibrium effect caused by surface and/or adsorbate packing interactions; kinetic effect caused by diffusing rates; quantum sieving associated with quantum effects. Thermal, geometric, and kinetic factors play prominent roles in these mechanisms. However, physisorption on exterior or interior surfaces of IRMOFs is one of the fundamental elements when concentration of the HE molecules is extremely low. Thus, it is important to understand physisorption processes occurring in the adsorption of HE molecules by IRMOF-8. We conducted our investigations with special emphasis on investigating the interactions of the HE molecules with the exterior surface of the IRMOF-8. Adsorption of the HE molecules starts at the exterior surface of IRMOF-8, and the physisorption will affect the overall efficiency and selectivity of the proposed explosive preconcentrator. Investigation of the interactions of HE molecules at the exterior of IRMOF also have technological implications. IRMOFs have been synthesized in bulk by solvothermal synthesis,[8,15−17] hydrothermal synthesis,[18] liquid diffusion method,[19] and deprotonating vapor diffusion.[20] Recently, microwave syntheses have been proven as a cost efficient technique in producing IRMOFs.[21,22] This technique typically produces nano- to microsized uniform IRMOF particles, resulting in large total exterior surface area. Therefore, investigating interactions of the HE molecules at IRMOF exterior surface is justified if the future preconcentrator technologies are to use mass produced IRMOF nanoparticles.

IRMOFs are studied for their potential applications in photonics, and photocatalysis and known to exhibit semiconductor behavior.[4,5] Changes in IRMOF electronic structures induced by the guest HE molecules could be exploited for direct, spectrophotometric methods for on-site, rapid detection technologies. Todays commonly used spectroscopic techniques provide high selectivity but lack sensitivity to detect trace amounts of HE molecules. Recently, Krause et al. showed that using adsorption-induced resonant frequency shift together with photothermal deflection spectroscopy has extremely high selectivity with a subnanogram limit of detection for vapor phase adsorbed explosives such as pentaerythritol tetranitrate (PETN), trinitrotoluene (TNT), and RDX.[23] Johnson-White et al. have demonstrated that periodic mesoporous organosilicas (PMO) with a porphyrin selectively adsorbs RDX and TNT over other analytes and exhibits unique changes in the spectrophotometric characteristics of the porphyrin, which can be observed by spectroscopic techniques.[24] In a similar spirit, we investigated electronic structures of the combined IRMOF-8−RDX system for signature changes induced by the guest HE molecules by analyzing contributions of the HE molecules to total density of states of the system.

We further extended our investigation by molecular dynamics simulations to explore how the physisorptions contribute to trapping configurations at finite temperature. Understanding the adsorption mechanisms of the HE molecules by IRMOF-8 at room temperature will provide important information for any practical use of IRMOF-8 as a preconcentrator for the explosives. The primary goal of MD simulations in this work is to obtain, starting from the physisorption configurations obtained at $T = 0$ K, an informed guess on the nature of adsorption mechanisms of HE molecules by IRMOF-8 at room temperature. It should also be noted that more comprehensive studies at finite temperature on similar systems have been performed by our collaborators using classical molecular dynamics; therefore, we refer readers to their work.[9]

We discuss our methodologies in section II, followed by discussions of results in sections III and IV. In the end, we briefly summarize our findings in section V.

II. Methods

We use the DFT quantum simulation code FIREBALL[25] for geometry optimization, electronic structure, calculation of interaction energies, and molecular dynamics simulations. The code uses compressed pseudoatomic orbitals to express the basis set.[26] Cut-off lengths result in a slight increase of orbital energies (0.15 Ryd excitation) due to the Fermi compression effect. We choose basis sets with chemically justified cutoff lengths for atomic wave functions.[27] Furthermore, the atomic orbitals for C, N, and O include double numerical orbitals (excited atomic orbitals) to provide additional degrees of freedom for calculating atomic interactions. Each orbital within our basis set is further refined by confining potentials to adjust tails of the orbital wave functions to an exponential form.[28] We use the Becke form of exchange interactions[29] with Lee−Yang−Parr correlation interactions[30] for all of the FIREBALL calculations presented here. Furthermore, we use the Horsefield functionals for the exchange correlation term to calculate interaction energies between the HE and IRMOF-8. Details of the methodology are extensively discussed elsewhere and we refer readers to relevant literature.[26,31]

We use experimental data[8] for IRMOF-8 lattice constant ($a_0 = 30.092$ Å) to construct the IRMOF-8 cage structure, extending it periodically in three dimensions, and local density approximation (LDA) for lattice relaxations at $T = 0$ K. For the lattice optimization, a primitive unit cell consisting of 142 atoms was used. This optimized lattice was used in examining interactions of the HE molecules with the IRMOF-8 structure.

The IRMOF-8 surface is modeled by a slab of three linker planes terminated at carboxyl groups along the (001) direction. The three linker planes satisfy mirror symmetry of the slab along the center plane and we chose supercell parameters so that the slab has a large vacuum at its top and bottom. The simulation supercell for the surface consists of 394 atoms.

For the interactions between the HE molecules and IRMOF-8, the combined structures have been optimized at $T = 0$ K first and energy calculations have been performed. Exploiting structural similarity between the IRMOF-1 and IRMOF-8, the HE molecules were originally placed at binding sites adjacent to the linkers and the connectors, as suggested by Michalkova et al.[32] To calculate the interaction energy for each combined structure, the IRMOF-8 cage and HE molecules are isolated for single point energy calculations. We define the binding as the given by

$$E_B = E_{(IRMOF+M)} - (E_{IRMOF} + E_M) \quad (1)$$

where $E_{(IRMOF+M)}$, E_{IRMOF}, and E_M are the total energies of the combined IRMOF+HE compound system, the IRMOF cage, and the adsorbate (the isolated RDX/TATP molecule), respectively.

For the MD simulations, we used a number−volume−temperature (*NVT*) ensemble with an explicit velocity Verlet

integrator, which uses the factorized Liouville operator to calculate time evolution of the atomic positions. The Hamiltonian is modified to a nonconservative system by adding a series of damped oscillator terms to the potential energy. Then a Nosé−Hoover chain thermostat was used to control the temperature,[33,34] allowing the system to cool/heat if the instantaneous kinetic energy is higher/lower than k_BT, where T is the desired temperature. Choosing the optimized IRMOF-8/HE structures at $T = 0$ K as starting configurations, we first increased the temperature to 300 K and then ran the MD simulations for 7 ps while tracking the position of the center of mass of the HE molecules. The physisorption configurations obtained at $T = 0$ K are not expected to remain at room temperature, and combination of long-range interactions such as steric hindrance, electrostatic, and van der Waals (vdW) forces are expected to become the main contributors. As a result, the trapping mechanism for the HE molecules at room temperature is of different nature than physisorption at $T = 0$ K and could be better described as molecular sieving or quantum sieving. We added empirical vdW terms with cutoff radius of 9.0 Å, and parameters C_6, α (polarizability), and R_0 for each atomic species for molecular-dynamics simulations at room temperature. As in schemes provided in refs 35 and 36, the dispersive energy is described by damped interatomic potentials of the form (C_6R^{-6}). Although it is known that the empirical vdW approach has its limitations, it has been successfully used in combination with DFT on many systems.[36−40] We tested the empirical vdW terms by calculations at 0 K for IRMOF-8/RDX system, for which contributions to interaction energies averaged at 2%. This suggests that vdW forces alone is not the dominant player for this system at room temperature.

MD simulations started from the configurations optimized at $T = 0$ K. The initial placements reduce transient time, during which the HE molecules migrate to their optimal positions. The IRMOF-8 atoms are fixed in space during the MD simulations, while the HE atoms had freedom to move. Effects of flexible IRMOF frame on adsorptions have been studied before and pointed to their role in accessing interiors of the cage by the guest molecules.[11,41,42] While we rendered the IRMOF-8 cage as a rigid structure to save computational time, charges in the entire system were allowed to settle self-consistently. Furthermore, we tracked the center of mass of the HE molecules during the molecular dynamics simulations to determine potential trapping configurations at room temperature.

III. Results

We optimized the IRMOF-8 structure at the LDA level with Sankey−Niklowski exchange correlation.[43] To calculate the IRMOF-8 electronic structure, integration was performed over the Brilloun zone using the Monkhorst−Pack mesh with 4 k points. Thr total electronic density of states and electronic band structure of the IRMOF-8 are shown in Figure 3a,b, respectively. The band gap is approximately 2.8 eV, which is significantly smaller than the band gap of 3.5 eV for IRMOF-1.[44] The conduction band is split in two regions, and the lower part has width of 209 meV. We will discuss changes in the electronic structures induced by adsorption of RDX/TATP molecules later.

We investigated seven possible RDX physisorption configurations by IRMOF-8, of which L1, and L2 represent 2,6-naphthalenedicarboxylate linker sites, and C1, C2, C3, C4, and C5 represent connector sites (Figure 4). We list the interaction energies in Table 1; the data show that configurations L1, L2, C4, and C5 are binding. Interactions of the HE molecules with the interior of IRMOF-8 can be viewed in two distinct classes

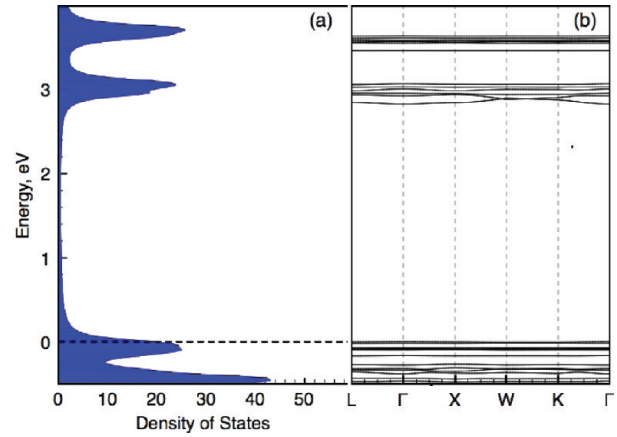

Figure 3. Electronic structure of IRMOF-8: (a) total density of states; (b) electronic band structure.

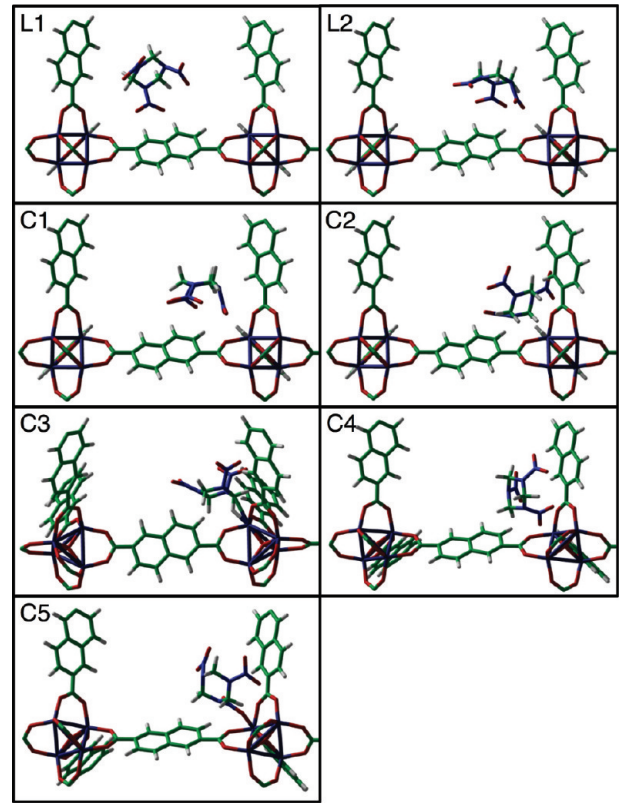

Figure 4. RDX physisorption configurations with IRMOF-8.

due to two different accessible volumes within the cage structure. Depending on the orientation of the NDC linkers, IRMOF-8 has either big or small cages in its periodic structure. Each cube in the IRMOF-8 cage has dimensions of 14.94 Å, and accessible volume for the big and small cages are spheres with diameters 21.13 and 15.62 Å, respectively. For the big cage, NDC linker planes are oriented tangent to the sphere of accessible volume, while the planes are perpendicular to the sphere in the small cage. In comparison, the RDX and TATP molecules span 6.03 and 7.43 Å, respectively, at their widest points. According to our calculations, all physisorption configurations occur in the bigger cage, while the unbound configurations C1, C2, and C3 occur in the smaller cage. Absence of physisorptions in the smaller cage indicates steric hindrance to the connector sites caused by the inward protruding NDC linkers. The HE molecules are relatively small compared to both big and small cages. However, orientation of the LDC

TABLE 1: Interaction Energies (kcal/mol) for RDX Physisorption Configurations at Interior and Exterior Surfaces of the IRMOF-8 Cage

	L1	L2	C1	C2	C3	C4	C5
IRMOF-8 interior	−5.30	−6.91	+9.21	+13.82	+32.49	−14.06	−9.45
IRMOF-8 exterior	+1.61	−4.61	+23.96	−2.76	+23.04	−10.60	+1.38

linkers in the small cage results in steric hindrance to connectors, reducing the overall number of potential physisorption sites. This is also consistent with results of our previous studies on IRMOF-1−RDX system, in which steric hindrance prevents physisorptions at connector sites in the periodic IRMOF-1 cage.

Effects of RDX in the electronic structure of IRMOF-8 are shown in Figure 5. Placing a molecule in each of the unit cells of the periodic IRMOF-8 cage is for simulation purposes only and amounts to an extremely high concentration of HE in real life scenario. However, it gives us a glimpse of how electronic structures of IRMOF-8 are affected by the explosive molecules and provides information for detection methods based on spectrometric techniques. Electronic structures of the RDX have been studied mostly for solid RDXs,[45−49] with an experimentally determined band gap of 3.4 eV.[50] Computational investigations of perfect RDX solid are known to produce band gap values ranging from 3.96 to 5.25 eV.[51,52] However, it has been revealed by Kuklja et al. that defects in the RDX crystal lead to narrowing of the band gap, resulting in values comparable with the experiment.[52] In our calculations, we obtained HOMO−LUMO gap of ∼3.1 eV for RDX molecule inside the periodic IRMOF-8 cage, which is 0.3 eV less than the experimental value. This difference is due to the LDA used in our DFT calculations, which is known to underestimate band gaps. In Figure 6, contributions of RDX to total density of states is color coded by red, while the total density of states is plotted in blue. In the IRMOF-8/RDX system, HOMO state of the RDX molecule appears in the gap region of IRMOF-8, reducing the band gap by 1.0−1.4 eV. This change of IRMOF-8 electronic structure, induced by the guest HE molecules, could be exploited in spectroscopic explosive detecting technologies. The top of the IRMOF-8 valence band becomes the HOMO level for the combined system and is associated with the organic linkers, while LUMO states are located mostly at NO_2 groups of the RDX that are closest to the IRMOF-8.

We find that physisorption interactions of RDX with the IRMOF-8 exterior surface differ from those with the interior. One of the configurations associated with the linker, L1, is an unbound site on the exterior surface. Interaction energies for configurations associated with connectors have also changed on the surface: C1, C2, and C3 configurations in the smaller cage are bound. The HOMO/LUMO states at the surface are now clustered around carbon atoms at the termination plane, and are not associated with the RDX molecule.

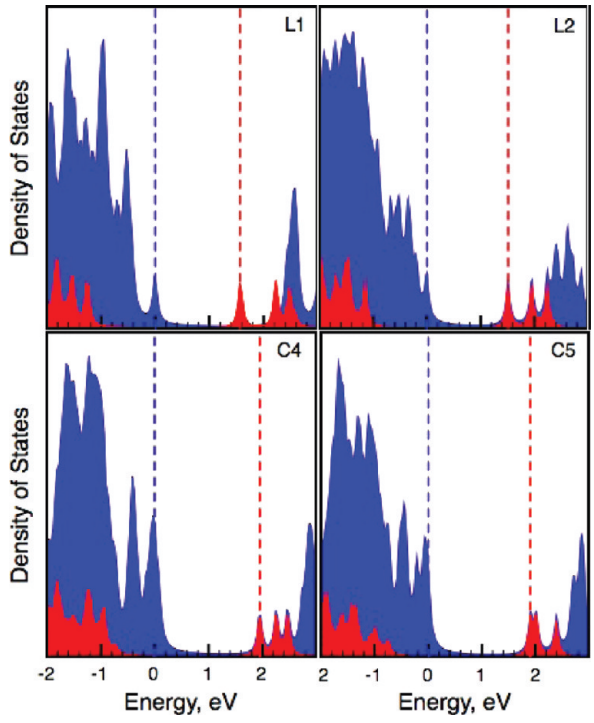

Figure 5. Electronic structures of bulk IRMOF-8−RDX combined system for physisorption structures L1, L2, C4, and C5. Total density of states (blue) and contributions from RDX molecules (red). The blue and red vertical dashed lines mark HOMO and LUMO states.

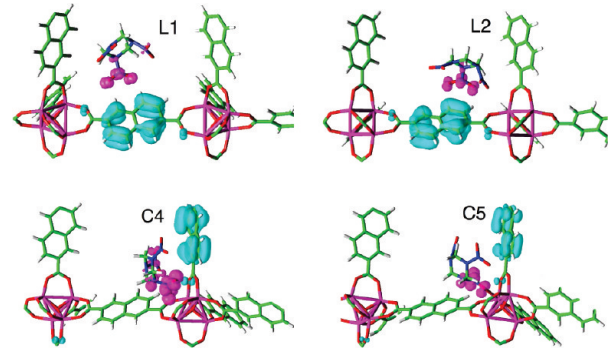

Figure 6. HOMO (blue) and LUMO (red) states of the IRMOF-8−RDX systems.

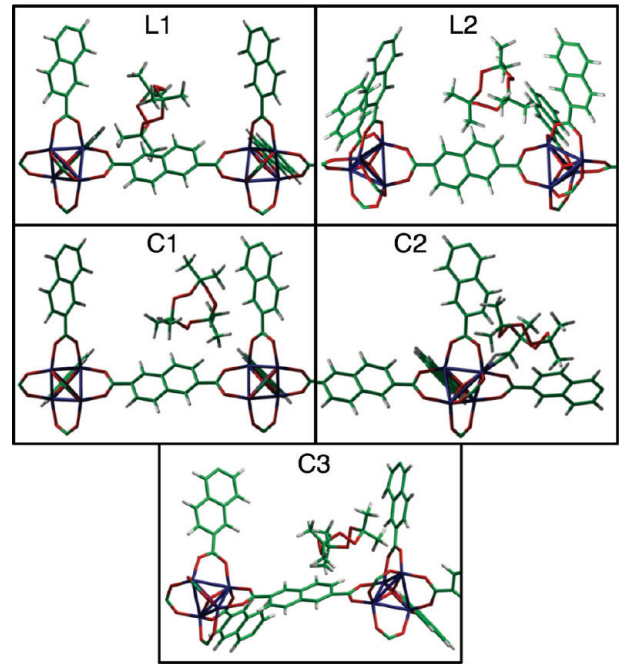

Figure 7. Initial configurations for TATP and IRMOF-8 physisorption studies.

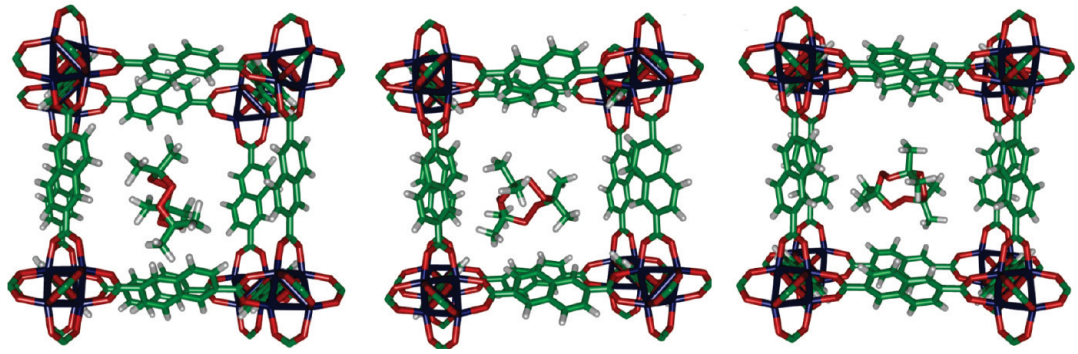

Figure 8. TATP stable configurations in the interior of IRMOF-8 cage at $T = 300$ K.

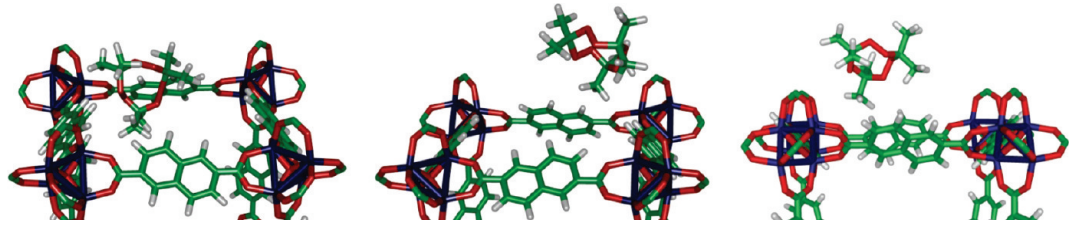

Figure 9. TATP stable configurations on the surface of IRMOF-8 at $T = 300$ K.

For the interactions of TATP molecule with IRMOF-8, we obtained no energetically feasible physisorption configurations despite having explored many initial configurations (Figure 7). We attribute this difference mainly to steric hindrances from the six methyl groups of TATP, and its relatively large size compared with RDX. Hydrogen atoms in the TATP methyl groups and IRMOF-8 NDC linkers have donated charges to their carbon neighbors, thus hindering physisorptions involving these atoms. The relatively bigger size and its geometry further prevent orbital interactions of the TATP molecule with IRMOF-8 connectors. In contrast, oxygen atoms of NO_2 groups of RDX molecule are electrically negative and provide more orbital interactions with the surrounding IRMOF-8 cage.

IV. HE/IRMOF-8 Interaction at Room Temperature

We performed constant temperature MD simulations at $T = 300$ K for each of the optimized configurations found at $T = 0$ K and observed dynamics of the HE molecules; the simulations ran for about 7 ps. The physisorption configurations obtained at $T = 0$ K are not expected to remain at room temperature, and long-range interactions such as steric hindrance, electrostatic, and quantum effects are expected to become main contributors. As a result, the trapping mechanism for the HE molecules found at room temperature is of a different nature than physisorption at $T = 0$ K and could be better described as molecular sieving or quantum sieving. The general picture is that the HE molecules dissociate from their 0 K physisorption sites and migrate toward the center of the cage at 300 K, which is the energetically favorable location as steric hindrances, and other long-range forces are minimized. For the RDX molecule, 7 ps MD simulations failed to result in stable trapping configurations. We have obtained three stable trapping configurations for TATP in the interior of the IRMOF-8 cage, at which the molecule resided over 60% of the 7 ps MD run (Figure 8), and kept its orientation with respect to the IRMOF-8 cage. This difference suggests a molecular sieving effect caused by differences in size and shape of the RDX and TATP molecules. The common feature of the TATP trapping configurations is that methyl groups form the nearest proximity to NDC groups of IRMOF-8 linkers with average distance of 6.8 Å. This distance is close to the sum of cutoff lengths used in the basis set, thus the trapping of the molecule could not be attributed to orbital interactions alone.

We have obtained a similar picture from MD simulations at $T = 300$ K on the exterior surface of the IRMOF-8, resulting in three stable configurations for TATP (Figure 9), and no trapping configuration for the RDX molecule. The long-range interactions that resulted in molecular sieving effects in the interior could also be causing the trapping of the TATP at the exterior surface.

V. Summary

In this paper, we explored physisorption interactions of the HE molecules RDX and TATP with both interior and exterior surfaces of IRMOF-8, and dynamics of the molecules at room temperature.

Investigations at $T = 0$ K resulted in four physisorption configurations of RDX in the interior of the IRMOF-8 cage. These physisorption configurations fall in the bigger cage, where steric hindrances from the IRMOF-8 cage are minimal. We have not found physisorption configurations for the TATP molecule despite exploring many different initial geometries. The TATP molecule features six methyl groups in its ends, and this feature makes it less favored for physisorption at linker sites of the IRMOF-8. On the other hand, the connector sites area is excluded from the interaction due to steric hindrances from the large NDC linkers of the IRMOF-8.

In our previous studies on the combined IRMOF-1−RDX system, we observed sa ystematic difference between interior and surface physisorptions, in which the exterior surface of IRMOF-1 interacts more strongly with the RDX molecule than the interior. The stronger physisorptions at the IRMOF-1 exterior are associated with connectors, which are largely inert sites for the RDX molecule in the interior due to steric hindrances. Also, interaction energies for physisorptions on IRMOF-1 linkers are largely unaffected at exterior or interior configurations. For the IRMOF-8−RDX system, there is no systematic difference between the interior and exterior interactions, suggesting that the larger NDC linkers provide more steric hindrances, preventing the RDX physisorption to the connectors. Weak physisorp-

TABLE 2: Interaction Energies (kcal/mol) for TATP Metastable Configurations at Interior and Exterior Surfaces of the IRMOF-8 Cage

	L1	L2	C1	C2	C3
IRMOF-8 interior	+6.00	+11.29	+17.74	+12.67	+35.48
IRMOF-8 exterior	+8.98	+14.06	+9.68	+12.67	+13.59

tions at the exterior connectors of IRMOF-8−RDX suggests that steric hindrances from the NDC linkers are still felt at the exterior of IRMOF-8.

At room temperature, the HE molecules migrate toward the energetically more favorable center of the cage at 300 K. We obtained three trapping configurations of TATP for both the interior and exterior of the IRMOF-8 but failed to obtain stable trapping configurations for the RDX molecule during 7 ps MD simulations. Our results show that long-range interactions become dominant factors at room temperature, giving rise to molecular sieving as the trapping mechanisms of the HE molecules by IRMOF-8.

To fully explore use of IRMOF-8 as explosive preconcentrator for RDX/TATP molecules, MD studies of the system at room temperature must be further extended, including comparative investigations with experiments and computational studies of other porous materials. Unfortunately, literature search failed to reveal reports of computational studies on interactions of these molecules with other porous materials such as zeolites and carbons at this stage.

Acknowledgment. We thank for Dr. D. Keffer, J. Leszczynski, and A. Michalkova for their insightful discussions. We gratefully acknowledge the financial support of National Science Foundation (NSF) under grant CMMI-0730207. Work at ORNL was performed under the auspices of the Division of Materials Science and Engineering, Office of Basic Energy Science of the U.S. Department of Energy. Also, we thank the Pittsburgh Supercomputing Center and WVNano for computing facilities.

References and Notes

(1) Rosi, N.; Eckert, J.; Eddaoudi, M.; Vodak, D.; Kim, J.; O'Keeffe, M.; Yaghi, O. *Science* **2003**, *300*, 1127–1129.
(2) Rowsell, J.; Yaghi, O. *Angew. Chem., Int. Ed.* **2005**, *44*, 4670–4679.
(3) Li, J.-R.; Kuppler, R. J.; Zhou, H.-C. *Chem. Soc. Rev.* **2009**, *38*, 1477–1504.
(4) Alvaro, M.; Carbonell, E.; Ferrer, B.; Llabres i Xamena, F. X.; Garcia, H. *Chem.−Eur. J.* **2007**, *13*, 5106–5112.
(5) Xamena, F. X. L. i.; Corma, A.; Garcia, H. *J. Phys. Chem. C* **2007**, *111*, 80–85.
(6) Sudik, A.; Millward, A.; Ockwig, N.; Cote, A.; Kim, J.; Yaghi, O. *J. Am. Chem. Soc.* **2005**, *127*, 7110–7118.
(7) Yaghi, O.; Li, G.; Li, H. *Nature* **1995**, *378*, 703–706.
(8) Eddaoudi, M.; Kim, J.; Rosi, N.; Vodak, D.; Wachter, J.; O'Keeffe, M.; Yaghi, O. *Science* **2002**, *295*, 469–472.
(9) Xiong, R.; Fern, J. T.; Keffer, D. J.; Fuentes-Cabrera, M.; Nicholson, D. M. *Mol. Simul.* **2009**, *35*, 910–919.
(10) Yaghi, O. M.; O'Keeffe, M.; Ockwig, N. W.; Chae, H. K.; Eddaoudi, M.; Kim, J. *Nature* **2003**, *423*, 705–714.
(11) Jakobtorweihen, S.; Verbeek, M.; Lowe, C.; Keil, F.; Smit, B. *Phys. Rev. Lett.* **2005**, 95.
(12) Sagara, T.; Klassen, J.; Ortony, J.; Ganz, E. *J. Chem. Phys.* **2005**, 123.
(13) Yang, R. T. *Adsorbents: Fundamentals and Applications*; John Wiley & Sons: Hoboken, NJ, 2003.
(14) *Gas Adsorption Equilibria, Experimental Methods and Adsoptive Isotherms*; Springer Science+Business Media: Boston, 2005.
(15) Chui, S.; Lo, S.; Charmant, J.; Orpen, A.; Williams, I. *Science* **1999**, *283*, 1148–1150.
(16) Dybtsev, D.; Nuzhdin, A.; Chun, H.; Bryliakov, K.; Talsi, E.; Fedin, V.; Kim, K. *Angew. Chem., Int. Ed.* **2006**, *45*, 916–920.
(17) Kosal, M.; Chou, J.; Wilson, S.; Suslick, K. *Nat. Mater.* **2002**, *1*, 118–121.
(18) Lin, W.; Wang, Z.; Ma, L. *J. Am. Chem. Soc.* **1999**, *121*, 11249–11250.
(19) Seo, J.; Whang, D.; Lee, H.; Jun, S.; Oh, J.; Jeon, Y.; Kim, K. *Nature* **2000**, *404*, 982–986.
(20) Smithenry, D.; Wilson, S.; Suslick, K. *Inorg. Chem.* **2003**, *42*, 7719–7721.
(21) Tompsett, G.; Conner, W.; Yngvesson, K. *Chemphyschem* **2006**, *7*, 296–319.
(22) Ni, Z.; Masel, R. I. *J. Am. Chem. Soc.* **2006**, *128*, 12394–12395.
(23) Krause, A. R.; Van Neste, C.; Senesac, L.; Thundat, T.; Finot, E. *J. Appl. Phys.* **2008**, 103.
(24) Johnson-White, B.; Zeinali, M.; Shaffer, K. M.; Patterson, J.; Charles, H.; Charles, P. T.; Markowitz, M. A *Biosens. Bioelectron.* **2007**, *22*, 1154–1162.
(25) Lewis, J.; Glaesemann, K.; Voth, G.; Fritsch, J.; Demkov, A.; Ortega, J.; Sankey, O. *Phys. Rev. B* **2001**, *64*, 195103.
(26) Sankey, O. F.; Niklewski, D. J. *Phys. Rev. B* **1989**, *40*, 3979–3995.
(27) Ortega, J.; Lewis, J. P.; Sankey, O. F. *Phys. Rev. B* **1994**, *50*, 10516.
(28) Jelinek, P.; Wang, H.; Lewis, J. P.; Sankey, O. F.; Ortega, J. *Phys. Rev. B* **2005**, *71*, 235101.
(29) Becke, A. D. *Phys. Rev. A.* **1988**, *38*, 3098.
(30) Lee, C.; Wang, W.; Parr, R. G. *Phys. Rev. B.* **1988**, *37*, 785.
(31) Sankey, O.; Demkov, A.; Windl, W.; Fritsch, J.; Lewis, J.; Fuentes-Cabrera, M. The application of approximate density functionals to complex systems. *Int. J. Quantum Chem.* **1998**, *69*, 327−340.
(32) Leszczynski, J.; Petrova, T.; Michalkova, A. Theoretical Study of RDX and TATP Interactions with MOF-5. Physical Science and Technology Conference, 2008.
(33) Nose, S. *J. Chem. Phys.* **1984**, *81*, 511–519.
(34) Hoover, W. *Phys. Rev. A* **1989**, *40*, 2814–2815.
(35) Grimme, S. *J. Comput. Chem.* **2004**, *25*, 1463–1473.
(36) Elstner, M.; Hobza, P.; Frauenheim, T.; Suhai, S.; Kaxiras, E. *J. Chem. Phys.* **2001**, *114*, 5149–5155.
(37) Wu, Q.; Yang, W. *J. Chem. Phys.* **2002**, *116*, 515–524.
(38) Dong, H.; Hua, S.; Li, S. *J. Phys. Chem. A* **2009**, *113*, 1335–1342.
(39) Williams, R. W.; Malhotra, D. *Chem. Phys.* **2006**, *327*, 54–62.
(40) Du, A.; Smith, S. *Nanotechnology* **2005**, *16*, 2118–2123.
(41) Forester, T.; Smith, W. *J. Chem. Soc., Faraday Trans.* **1997**, *93*, 3249–3257.
(42) Fletcher, A.; Thomas, K.; Rosseinsky, M. *J. Solid State Chem.* **2005**, *178*, 2491–2510.
(43) Sankey, O. F.; Niklewski D. J.; Drabold, D. A.; Dow, J. D. *Phys. Rev. B* **1990**, *41*, 12750−12759.
(44) Fuentes-Cabrera, M.; Nicholson, D.; Sumpter, B.; Widom, M. *J. Chem. Phys.* **2005**, 123.
(45) Kuklja, M.; Kunz, A. *J. Appl. Phys.* **1999**, *86*, 4428–4434.
(46) Kuklja, M.; Kunz, A. *J. Phys. Chem. B* **1999**, *103*, 8427–8431.
(47) Kuklja, M.; Stefanovich, E.; Kunz, A. *J. Chem. Phys.* **2000**, *112*, 3417–3423.
(48) Kuklja, M.; Kunz, A. *J. Appl. Phys.* **2001**, *89*, 4962–4970.
(49) Kunz, A. *Phys. Rev. B* **1996**, *53*, 9733–9738.
(50) MARINKAS, P. *J. Lumin.* **1977**, *15*, 57–67.
(51) Kuklja, M. M.; Kunz, A. B. *J. Phys. Chem. Solids* **2000**, *61*, 35–44.
(52) Kuklja, M.; Aduev, B.; Aluker, E.; Krasheninin, V.; Krechetov, A.; Mitrofanov, A. *J. Appl. Phys.* **2001**, *89*, 4156–4166.

JP906192G